Energy & Environmental Science

ROYAL SOCIETY OF CHEMISTRY

PAPER

View Article Online
View Journal | View Issue

Cite this: *Energy Environ. Sci.*, 2020, **13**, 3064

Interfacial water shuffling the intermediates of hydrogen oxidation and evolution reactions in aqueous media†

Ershuai Liu,[a] Li Jiao,[b] Jingkun Li,‡[a] Thomas Stracensky,[a] Qiang Sun,[a] Sanjeev Mukerjee[a] and Qingying Jia *[a]

Received 2nd June 2020,
Accepted 5th August 2020

DOI: 10.1039/d0ee01754j

rsc.li/ees

The kinetics of the hydrogen oxidation and evolution reactions (HOR/HER) of platinum in aqueous solutions remains elusive, partly because of the lack of means to explore the surface–electrolyte interface. Herein, we probe this interface by utilizing surface transition metals (TMs), carbon monoxide, alkali metal cations (AM^+), and heavy water in combination with *in situ* X-ray absorption spectroscopy. It was found that the surface TMs in the metallic phase may boost the HOR kinetics of Pt in alkali by hosting the interfacial water with the oxygen-down orientation that removes the adsorbed hydrogen on Pt neighbors. Furthermore, surface TMs in either metallic or hydroxide phases improve the HER kinetics of Pt by hosting the hydroxyl generated from water dissociation so it can be desorbed by the interfacial water coordinated to AM^+. The roles of interfacial water in shuffling the HOR/HER intermediates throughout the interface are supported by kinetic isotope effects.

Broader context

Recent studies highlight the importance of double-layer interfaces in many electrochemical reactions such as hydrogen oxidation/evolution reactions (HOR/HER) and oxygen reduction/evolution reactions (ORR/OER). However, lack of means probing the interface during reactions forbids clear understandings of reaction mechanisms, which in turn impedes rational design of catalysts. This work demonstrates a method probing the interface of the HOR/HER of Pt-based catalysts *in situ*, which reveals the essential and complex roles of interfacial water on the HOR/HER kinetics of Pt-based catalysts in aqueous solutions. New mechanisms of the HOR/HER of Pt are proposed based on these new findings. We believe this work has broad impacts in three aspects: (1) the new HOR/HER mechanisms proposed here may guide rational design of new HOR/HER catalysts for alkaline exchange membrane fuel cells; (2) the roles of interfacial waters revealed here can be extended to many other reactions; and (3) the new method to probe the reaction interface established here is applicable to other reactions.

1. Introduction

Hydrogen oxidation and evolution reactions (HOR/HER) are the electrochemical transformations between H_2 and water. Clear understanding of the HOR/HER kinetics holds the key for efficient consumption of H_2 in fuel cells and production of H_2 from water in electrolyzers. In addition to their practical significance, HOR/HER are the most fundamentally important reactions in electrochemistry. Studies of the HOR/HER kinetics in acidic solutions led to the discovery of two underlying principles in electrochemistry: the Butler–Volmer equation[1] and Sabatier's principle.[2] The HOR/HER activities of a broad range of elements in acidic solutions exhibit a volcano trend as a function of the metal–H binding energy (E_{M-H}), with Pt sitting near the top as per the Sabatier principle.[3] However, this coherent picture of the HOR/HER kinetics in acid is not fully applicable when extending to high pH media. The HOR/HER rates of several transition metals (TMs) including Rh, Pd, Ir, Pt, and Au are all slower in alkali than in acid, irrespective of their E_{M-H}(s).[4] These results indicate the breakdown of the Sabatier principle in the HOR/HER kinetics across a wide pH range. The sluggish HOR/HER kinetics of Pt in alkaline solutions, a seemingly simple phenomenon, remains one of the most important puzzles in electrochemistry.

Hitherto, several hypotheses have been proposed to account for the pH dependence of the HOR/HER kinetics of Pt. Yan *et al.*[5–7] ascribed it to the pH-dependent E_{Pt-H}, and later to the apparent E_{Pt-H} (E_{Pt-H}(app) = $E_{Pt-H} - E_{Pt-H_2O}$) that also takes the binding towards interfacial water into consideration (HBE theory). By this theory, as the E_{Pt-H_2O} weakens with increasing pH, the E_{Pt-}

[a] *Department of Chemistry and Chemical Biology, Northeastern University, Boston, Massachusetts, 02115, USA. E-mail: q.jia@northeastern.edu*
[b] *Department of Chemical Engineering, Northeastern University, Boston, Massachusetts, 02115, USA*

† Electronic supplementary information (ESI) available. See DOI: 10.1039/d0ee01754j

‡ Present address: Institut Charles Gerhardt Montpellier, UMR 5253, CNRS, Université Montpellier, ENSCM, Place Eugène Bataillon, 34095 Montpellier Cedex 5, France.

$_H$(app) becomes stronger and leads to slower HOR/HER kinetics of Pt. Moreover, this argument is supported by the recent computational work by Goddard *et al.*[8] In contrast, Markovic *et al.*[9,10] ascribed the slower HER kinetics of Pt in alkali to the high energy barrier of H_2O dissociation to generate H_{ad}, and slower HOR to the high energy barrier of bringing OH^- from the electrolyte onto the surface to react with H_{ad} (bifunctional theory). Koper *et al.*[11,12] later ascribed the pH-dependence of the HOR/HER kinetics of Pt to the pH-dependent potential of zero free charge (pzfc). As the pzfc shifts away from the HOR/HER potential with increasing pH, interfacial water becomes less flexible and requires higher energy penalties to accommodate charge transfer throughout the double-layer interface (pzfc theory). The key discrepancy within these hypotheses lies in the roles of interfacial water. The sluggish HOR/HER kinetics of Pt in alkaline solutions has been explained as either the interfacial water binds to the Pt electrode too weakly (HBE theory), or too difficult to break/form (bifunctional theory), or too rigid to reorient (pzfc theory).

The HOR/HER kinetics of Pt not only slows down when shifting from acidic to alkaline solutions but also becomes sensitive to surface structures and alkali metal cations (AM^+). For example, the Pt(110) facet exhibits superior HOR/HER kinetics to Pt(111) in alkali.[13] The HOR/HER rates of Pt surfaces other than Pt(111) decrease in the sequence of LiOH > NaOH > KOH.[14,15] Meanwhile, the HER of stepped Pt surfaces improves with increasing AM^+ concentration whereas the HOR rate slightly decreases.[14,16–18] However, these cation effects are absent for Pt(111).[18,19] The HOR/HER kinetics of Pt in alkaline solutions can be modulated by the surface TMs and the modulation is highly sensitive to the TM identity. For instance, surface Ru dramatically improves the HOR/HER of Pt in alkali,[9,19,20] while surface Ni markedly improves the HER[9,11,14,15] but only marginally improves the HOR.[14,15] In contrast, surface Mn and Co exclusively promote the HER.[15] Until now a singular theory that is compatible with all these observations has been missing.

Inspired by the high sensitivities of the HOR/HER kinetics of Pt to the TM identity in alkali, herein we probe the Pt electrode/electrolyte interface by depositing a variety of TMs onto Pt surfaces and monitoring their redox-controlled interactions with the HOR/HER intermediates and interfacial water *via in situ* X-ray absorption spectroscopy (XAS). Carbon monoxide (CO) stripping experiments with varied AM^+ concentrations are conducted to facilitate correlating the redox-controlled interactions to the TM-induced changes of the HOR/HER kinetics of Pt. Upon establishment of the correlations we conclude that interfacial water catalyzes the HOR/HER of Pt *via* shuffling the reaction intermediates throughout the interface, and the pH, AM^+, and surface TM affect the HOR/HER kinetics of Pt by affecting the shuffling capability of interfacial water. The participation of interfacial water in the HOR/HER of Pt is then verified by kinetic isotope effect (KIE) studies in alkaline solutions.

2. Results and discussion

To investigate the effect of surface TM on the HOR/HER kinetics of Pt in alkaline solution, the Pt polycrystalline electrode is immersed in a TM solution (such as $Mn(ClO_4)_2$) following our previous protocol for surface TM deposition.[14] The TM coverage on the electrode can be tuned *via* varying the concentration in solution.[14,20] The HOR/HER polarization curves of the bare and deposited electrode (denoted as TM@Pt) are obtained by rotating disk electrode (RDE) in H_2-saturated 0.1 M KOH electrolyte (99.99%). It is found that the TM-induced changes to the HOR/HER rates of Pt vary dramatically with the TM identity. The Ru@Pt and Ni@Pt improve both the HOR/HER rates of Pt (Fig. 1a and b), in agreement with literature.[9–11,19,20] In particular, the Ni-induced and Ru-induced HOR improvement gradually vanishes as the potential increases to 0.1 V and 0.15 V (all potentials here are *versus* the reversible hydrogen electrode), respectively. For Mn@Pt (Fig. 1c), Fe@Pt (Fig. S1a, ESI†), and Co@Pt (Fig. 1d) the HER rate increases but HOR rate decreases, consistent with Tang *et al*'s recent results.[15] Taking the Co@Pt as a representative example, the limiting current density (Fig. 1d) and the cyclic voltammetry (CV) (Fig. S2a, ESI†) remain nearly unchanged when immersing the Pt electrode in a 20 μM $Co(ClO_4)_2$ solution, indicating a negligible coverage of Co on the Pt surface. Despite the minimal Co coverage, the HER rate of Pt improves dramatically, which verifies that the surface Co does promote the HER kinetics of Pt. On the other hand, the trivial decrease of the HOR rate suggests that the surface Co has negligible effects on the HOR kinetics of Pt/C. As the concentration of $Co(ClO_4)_2$ increases to 100 μM, the Pt surface is largely blocked by Co as reflected by the marked drop of the underpotential-deposited hydrogen (H_{UPD}) charge (Fig. S2a, ESI†). Consequently, both the HOR/HER rates decrease. For Cu@Pt, the HOR/HER rates of Pt decrease slightly with 20 μM Cu^{2+} and decrease further with increasing Cu^{2+} concentration (Fig. 1e). This result indicates that the surface Cu has negligible effects on the HOR/HER kinetics of Pt. Finally, selective improvement of the HOR of Pt without improving the HER has not been reported hitherto (Fig. 1f).

No current theory can fully account for all the observed TM-induced changes of the HOR/HER kinetics of Pt in alkali, especially the potential dependent Ni/Ru-induced HOR improvement. To understand why different surface TMs affect the HOR/HER kinetic of Pt so differently (Fig. 1f), we conducted *in situ* XAS at the K-edge of these TMs@Pt, plus Ru/C (~6 nm, ETEK, 60 wt%), and Pt_1Ru_1/C alloy (ETEK, 29.1 wt%) during the HOR/HER in an H_2-saturated 0.1 M KOH electrolyte. As the potential increases, the X-ray absorption near edge structure (XANES) spectra of all the TMs shift to higher energy, approaching those of the (hydr)oxide standards (Fig. 2a–e). These trends indicate the progressive oxidation of the TMs, but to distinctly different extents. The changes in the bulk-average oxidation state of these TMs with increasing potentials can be quantitatively compared (Fig. 2f) by choosing the energy at which the XANES spectrum is at 0.3 (E_{edge}) relative to those of the standards (STDs) to represent the oxidation state: $(n \times (E_{edge}(TM) - E_{edge}(STD^{0+}))/((E_{edge}(STD^{n+}) - E_{edge}(STD^{0+}))$, wherein n^+ represents the valence of the STD (+2 for $Ni(OH)_2$), given that the oxidation state of TMs is nearly linearly related to the E_{edge}.[21] A typical choice of 0.5 for the E_{edge} is impractical for some 3d TMs since their XANES spectra converge around 0.5 as seen for the Co@Pt case in Fig. 2a and Ni@Pt case in Fig. S3, ESI†).

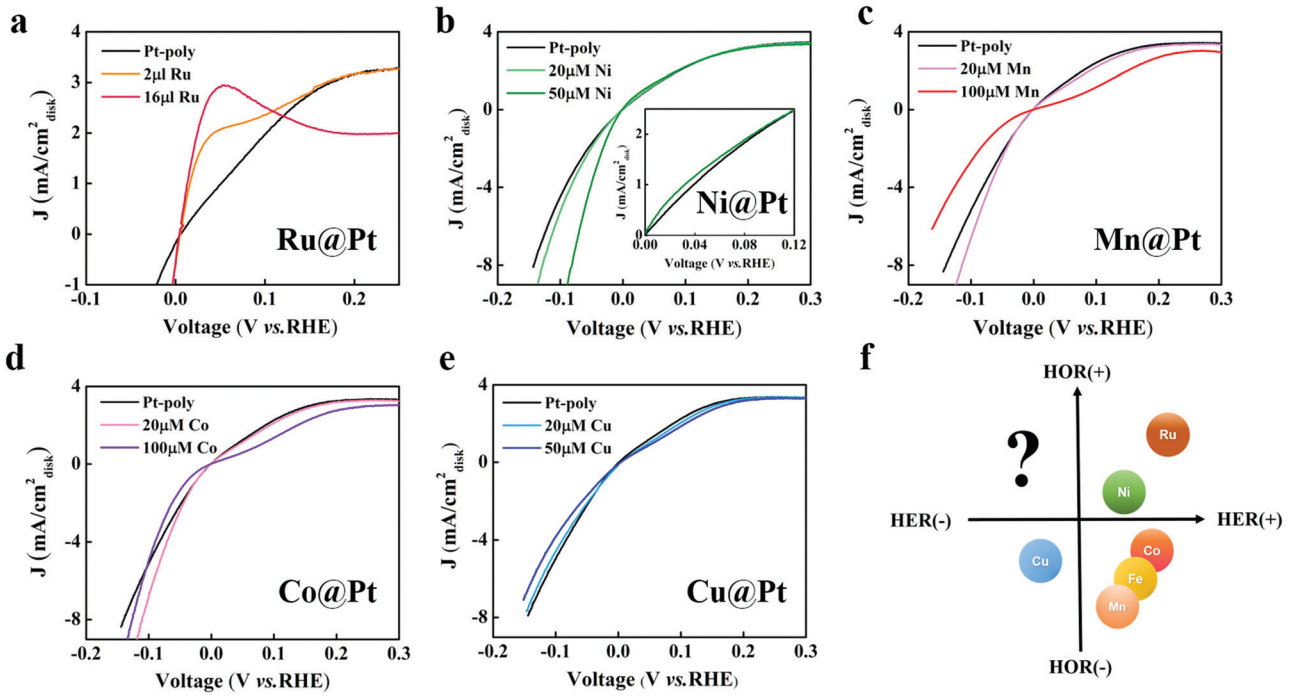

Fig. 1 The iR-corrected HOR/HER polarization curves of the Pt polycrystalline electrode with/without surface deposition of (a) Ru, (b) Ni (zoomed HOR region present in the inset), (c) Mn, (d) Co, and (e) Cu in an H_2-saturated 0.1 M KOH electrolyte at room temperature. Scan rate: 10 mV s^{-1}. Rotation rate: 2500 rpm. (f) Summary of TM-induced changes of the HOR/HER kinetics of Pt in the Cartesian coordinate system.

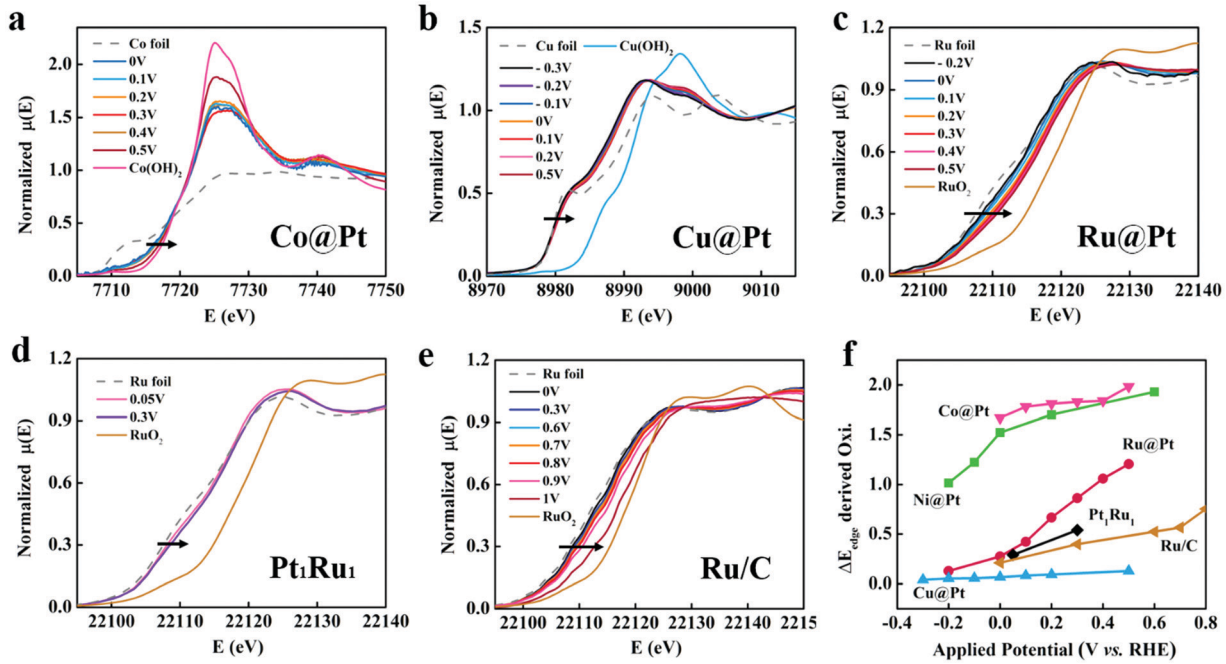

Fig. 2 K-Edge XANES spectra of the (a) Co@Pt, (b) Cu@Pt, (c) Ru@Pt, (d) Pt_1Ru_1/C alloy, (e) Ru/C as a function of applied potentials collected in an H_2-purged 0.1 M KOH electrolyte. (f) The oxidation states of TMs derived from the E_{edge} acquired from (a–e), and of Ni from our previous work with the full dataset provided in Fig. S3 (ESI†).[14]

The bulk-average oxidation state of Co@Pt is close to +2 at positive potentials, whereas that of Cu@Pt remains nearly zero throughout the potential range of −0.3 to 0.5 V (Fig. 2f). These results indicate that the Co@Pt is predominately in the form of (hydr)oxide at positive potentials, whereas the Cu@Pt remains largely in the metallic phase up to 0.5 V. Neither of these two elements exhibit clear redox transitions within the HOR potential range. In contrast, the Ni@Pt exhibits a clear redox transition

between $Ni/Ni(OH)_2$ as we showed previously.[14] The $Ni(OH)_2$ dominates at positive potentials and is gradually reduced to metallic Ni^0 as the potential shifts negatively below 0 V (Fig. 2f). This redox transition agrees with the $Ni/Ni(OH)_2$ redox potential of 0.05 V in alkali.[22,23] Similar to the Ni@Pt, the Ru@Pt is also redox-active within the HOR/HER potential region (Fig. 2c). Metallic Ru^0 is the dominant phase at −0.2 V with a bulk-average oxidation state of 0.13. As the potential increases to 0.5 V it is gradually oxidized reaching a bulk-average oxidation state of 1.2 (Fig. 2f). Similar trends are also observed on the Pt_1Ru_1/C (Fig. 2d) and Ru/C (Fig. 2e), but less steep because a significant fraction of Ru is buried in the core in the form of electroinactive Ru^0. The oxidation state of Ru/C rises gradually before 0.8 V and sharply beyond with increasing potentials (Fig. 2e and Fig. S4, ESI†), which is in line with the electrochemical measurements of a reversible $Ru/Ru(OH)_3$ transition between 0.2–0.8 V, followed by the redox transition of $Ru(OH)_3/RuO_2$ at 0.94 V.[24–26] These results together show that the phases and redox behaviors of TMs@Pt are distinctly different within the HOR/HER potential range.

The Fourier transform of the extended X-ray absorption fine structure (FT-EXAFS) spectra of the Co@Pt and Cu@Pt agree well with their XANES spectra. The FT-EXAFS of the Co@Pt is dominated by the Co–O (∼1.5 Å) and Co–Co (∼2.8 Å) peaks within the potential range of 0.1–0.5 V, whereas the Co–Co peak around 2.1 Å present in the Co foil is absent (Fig. 3a). The EXAFS fittings confirm that the bond lengths of Co–O and Co–Co of the Co@Pt at positive potentials are comparable to those of $Co(OH)_2$ (Fig. S5 and Table S1, ESI†), quantitatively verifying the predominate $Co(OH)_2$ phase in Co@Pt within the HOR potential region. Conversely, the FT-EXAFS spectra of the Cu@Pt exhibit a prominent Cu–Cu peak around 2.1 Å overlapping that

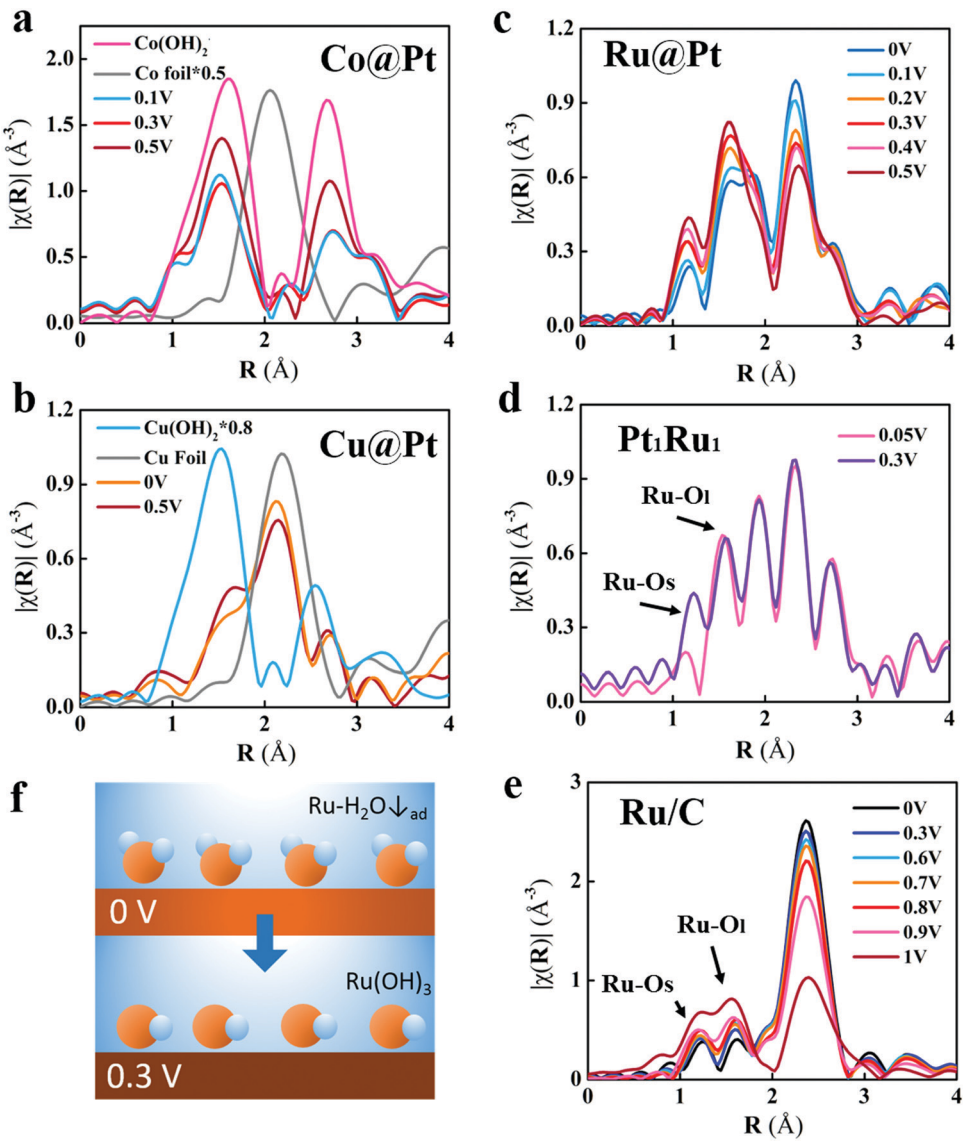

Fig. 3 K-Edge FT-EXAFS spectra of the (a) Co@Pt, (b) Cu@Pt, (c) Ru@Pt, (d) Pt_1Ru_1/C, and (e) Ru/C as a function of applied potentials collected in an H_2-purged 0.1 M KOH electrolyte. (f) Illustration of the redox transition from Ru^0–$H_2O\downarrow_{ad}$ to $Ru(OH)_3$ as the potential increases from 0 V to 0.3 V.

of the Cu foil (Fig. 3b) throughout the potential range from −0.3 V to 0.5 V, which verifies the metallic Cu^0 as the dominant phase in the Cu@Pt during the HOR/HER. A small Cu–O peak around 1.5 Å overlapping that of $Cu(OH)_2$ is discernible at positive potentials. This signifies the mild oxidation of Cu^0, consistent with the minor XANES shift.

The FT-EXAFS spectra of the Ru@Pt at all potentials exhibit five FT-EXAFS peaks within the range of 1–3 Å (Fig. 3c). These peaks are also observed in the Pt_1Ru_1/C (Fig. 3d),[27] and can be fitted with a Ru–Pt alloying model plus a Ru–O_x model with a short Ru–O bond (Ru–O_s) and a long Ru–O bond (Ru–O_l). The two Ru–O peaks are also present in the FT-EXAFS spectra of Ru/C, together with a sharp Ru–Ru peak around 2.4 Å (Fig. 3e). As the potential increases, the intensities of both Ru–O peaks increase, while the Ru–Ru and/or Ru–Pt peak intensities decrease. This trend indicates the progressive oxidation of the metallic Ru^0 phase with increasing potentials, consistent with the XANES results.

The bond lengths of the Ru–O_s and Ru–O_l bonds are determined to be ∼1.80 Å and ∼2.03 Å of all the three Ru-samples by fitting their FT-EXAFS spectra (Tables S2–S4, ESI†). The co-presence of metal–oxygen bonds with two different bond lengths, and particularly the ultra-short bond length of ∼1.80 Å are salient features of octahedral metal compounds subject to Jahn–Teller distortion,[28,29] for which the short and long bonds are associated with the axial and equatorial oxygen atoms, respectively. We therefore assign the Ru–O_s peak to the axial Ru–O bonds in $Ru(OH)_3$. The minimal Ru–O_s peaks at 0 V for all three Ru-samples in association with insignificant coordination numbers in comparison to fitting uncertainties (Tables S2–S4, ESI†) indicate the minimal amounts of $Ru(OH)_3$ at 0 V, which agrees with their XANES spectra that signify Ru^0 is the dominant phase at 0 V. However, the Ru–O_l peaks of the Ru@Pt and Pt_1Ru_1/C are prominent at 0 V, in association with significant coordination numbers of 1.9 ± 0.9 and 1.2 ± 0.4 respectively. They cannot be exclusively assigned to the equatorial Ru–O bonds in $Ru(OH)_3$ as its content at 0 V is only ∼9% as estimated from the E_{edge}-derived bulk average oxidation state of ∼0.27 (Fig. 2f). We instead assign them to the bond between the metallic Ru^0 and the O from the specifically adsorbed water with the O pointing toward the electrode (denoted as $H_2O{\downarrow_{ad}}$) as depicted in Fig. 3f. This assignment is further supported by the fitting result that the Ru–O_l bond distance is comparable to that of the Ru–H_2O bonds (2.04 ± 0.01 Å) in the $RuCl_3$ solution (Table S5, ESI†). The Ru^0–$H_2O{\downarrow_{ad}}$ binding configuration has been conceived theoretically and later observed experimentally on Ru(0001) under vacuum.[30–32] The H_2O_{ad} was also identified on the surface of nanoscale Ru-plates within the potential range of 0–0.2 V in both acid and alkaline solutions *via* electrochemical quartz crystal microbalance (EQCM):[24,25]

$$Ru^0 + H_2O \leftrightarrow Ru^0\text{–}H_2O{\downarrow_{ad}} \quad (1)$$

followed by the oxidation of Ru^0–$H_2O{\downarrow_{ad}}$ forming $Ru(OH)_3$ passivation layers as the potential increases to 0.8 V (Fig. 3f).

The potential-triggered redox transition of the Ru@Pt is clearly correlated to the potential dependent Ru-induced HOR improvement of Pt. The HOR improvement is substantial at 0 V when the surface Ru is dominated by Ru^0–$H_2O{\downarrow_{ad}}$. It gradually vanishes as the Ru^0–$H_2O{\downarrow_{ad}}$ gradually transforms to $Ru(OH)_3$ with increasing potentials. This correlation suggests that it is the Ru^0–$H_2O{\downarrow_{ad}}$ rather than $Ru(OH)_3$ that improves the HOR of Pt. We accordingly propose that the Ru^0 promotes the HOR of Pt by attracting H_2O from the electrolyte onto the surface in the orientation of $H_2O{\downarrow}$ (eqn (1)). The $H_2O{\downarrow_{ad}}$ subsequently removes the H_{ad} on the Pt neighbor through the L–H mechanism:

$$Pt\text{–}H_{ad} + Ru^0\text{–}H_2O{\downarrow_{ad}} \leftrightarrow Pt + Ru^0 + H_3O^+ + e^- \quad (2)$$

This reaction mechanism is further supported by the HOR kinetics of Ru/C. The HOR rate of Ru/C increases as the potential increases from 0 V to 0.2 V, and then gradually reduces to zero as the potential increases to 0.6 V (Fig. S12, ESI†). The Ru/C surface is dominated by Ru^0 below 0.2 V, and the HOR proceeds *via* the L–H mechanism between Ru^0–H_{ad} and Ru^0–$H_2O{\downarrow_{ad}}$, analogous to eqn (2). As the potential further increases, the Ru^0–$H_2O{\downarrow_{ad}}$ transforms to $Ru(OH)_3$ that passivates the surface, resulting in the reduction of the HOR limiting current to zero.

Our new argument contradicts the previous one that ascribed the Ru-induced HOR improvement of Pt to the Ru-induced change of the $E_{Pt\text{–}H}$ *via* electronic effects.[33–35] The Ru–Pt alloying phase is indeed detected by EXAFS in Ru@Pt. However, it largely preserves up to 0.5 V as evidenced by the nearly constant Ru–Pt coordination number of ∼2.7 with increasing potentials (Table S2, ESI†). Attributing the improved HOR activity to the Ru–Pt alloying phase is thus incompatible with the vanishing of the Ru-induced HOR improvement of Pt as the potential increases to 0.2 V (Fig. 1a).

This argument is also applicable to other TMs@Pt. Similar to Ru@Pt, the potential dependent HOR improvement of Ni@Pt up to 0.1 V (Fig. 1b) can be related to the presence of Ni^0 at 0 V and its disappearance at higher potentials,[14] or essentially the Ni/$Ni(OH)_2$ redox potential of 0.05 V.[22,23] No HOR improvement is observed on Co@Pt which is dominated by $Co(OH)_2$ within the HOR potential region. This is also the case of the Fe@Pt and Mn@Pt which have even higher oxophilicity or stronger binding energy towards oxygen ($E_{M\text{–}O}$) and thus lower redox potentials.[36] On the other hand, the Cu@Pt is incapable of binding $H_2O_{ad}{\downarrow}$ before Pt reaches the HOR mass transport limit by 0.25 V[37] owing to the weak $E_{Cu\text{–}O}$, as reflected by the statistically insignificant XAS signals of Cu–$H_2O_{ad}{\downarrow}$. Surface Cu thus cannot improve the HOR of Pt.

The sum of eqn (1) and (2) gives the Volmer step of Pt in acid:

$$Pt\text{–}H_{ad} + H_2O \leftrightarrow Pt + H_3O^+ + e^- \quad (3)$$

Upon the migration of the hydronium into the electrolyte and reacting with OH^-, eqn (3) transforms to the Volmer step in alkali:

$$Pt\text{–}H_{ad} + OH^- \leftrightarrow Pt + H_2O + e^- \quad (4)$$

This notion implies that the Volmer step of Pt in acid and alkaline is essentially the same (eqn (3)). The step in eqn (3) is kinetically slow for Pt in alkali because it requires bringing the $H_2O{\downarrow}$ with the negatively charged O facing towards the negatively charged surface.[11] The interfacial electric field has been estimated to be $\sim 10^8$ V m^{-1} at pH 7, and even stronger at higher pH.[38] Surface adsorption of the water with the O facing away from the electrode ($H_2O{\uparrow}$) is thus more energetically favorable than that of $H_2O{\downarrow}$, but the $H_2O{\uparrow}$ cannot react with H_{ad} forming hydronium.[39]

The redox-active behavior of Ru within the HOR kinetic region of Pt manifests its ability to attract and host $H_2O\downarrow$ (eqn (1)) against the electric field, thereby promoting the HOR kinetics of Pt in alkali. As the pH decreases, the pzfc shifts negatively to lower potentials, and the Pt surface becomes less negatively charged until reaching nearly neutral at pH = 1.[11,38] Consequently, the interfacial $H_2O\downarrow$ experience weaker electric field with decreasing pH, and the HOR kinetics of Pt becomes faster. Therefore, the pH-dependence of the HOR kinetics of Pt originates from the pH-dependent pzfc as proposed by Koper *et al.*[11] or electric field that dictates the orientation of interfacial water.[39]

The new notion indicates that the OH^- does not participate in the rate-determining step (rds) of the Pt HOR in alkali. This conflicts with the bifunctional mechanism wherein the H_{ad} is removed by the "reactive OH_{ad}" hosted by either TM^0 or $TM(OH)_x$, as originally proposed by Markovic *et al.* and later by us based on *in situ* XAS observation of OH_{ad} on the surface Ru of a Pt_1Ru_1/C alloy.[9,20,40] The presence of OH_{ad} on the surface was also observed on all TMs@Pt except for Cu@Pt (Fig. 2f), but only Ru@Pt and Ni@Pt show improved HOR kinetics. These observations indicate that the presence of surface OH_{ad} does not necessarily mean it participates the HOR, that is, it may not be the "reactive OH_{ad}". To trace the reactive OH_{ad} on the TM@Pt electrodes we conducted CO stripping experiments on them (except for Ru that is poisoned by CO[41]) as per the bifunctional reaction:[10,42] $TM^0/TM(OH)_x$–OH_{ad} + Pt–CO_{ad} ↔ $TM^0/TM(OH)_x$ + Pt–$COOH_{ad}$. All the surface TMs negatively shift the CO stripping peak of Pt towards lower potentials, indicating early adsorption of OH^- onto the surface as compared to the bare Pt electrode (Fig. 4a). Despite this, the CO stripping of the Ni@Pt does not initiate until 0.3 V (Fig. 4a), indicative of the absence of the reactive OH_{ad} below 0.3 V. Therefore, the surface Ni-induced HOR improvement up to 0.1 V cannot be ascribed to the OH_{ad}. Moreover, the OH_{ad}-based bifunctional mechanism is incompatible with the observations that the surface Mn does not improve the HOR of Pt despite that the CO oxidation initiates at lower potentials on Mn@Pt than on Ni@Pt (Fig. 4a); and the Ni/Ru-induced HOR improvements gradually diminish with increasing potential, although increasing potential favors OH^- adsorption. Our argument agrees with the recent kinetic study by Tang *et al.*[43] that rules out the participation of OH_{ad} in the HOR kinetics of Pt.

While the OH^- is unrelated to the HOR kinetics of Pt in alkali, the ones generated from water dissociation must be related to the HER kinetics. We previously proposed that the removal of OH_{ad} into the bulk electrolyte is the rds of the HER of Pt in alkali.[14] This step can be promoted by the surface TM such as Ni that hosts OH_{ad} to trigger the hard–soft acid–base (HSAB) mechanism:

$$TM^0/TM(OH)_x\text{–}OH_{ad}\text{–}[AM(H_2O)_x]^+ + e^- \leftrightarrow TM^0/TM(OH)_x + OH^-\text{–}[AM(H_2O)_x]^+ \quad (5)$$

together with the water molecules coordinated to AM^+ ($[AM(H_2O)_x]^+$) that shuffles the OH_{ad} out to the bulk electrolyte. This HSAB mechanism is further strengthened by the CO

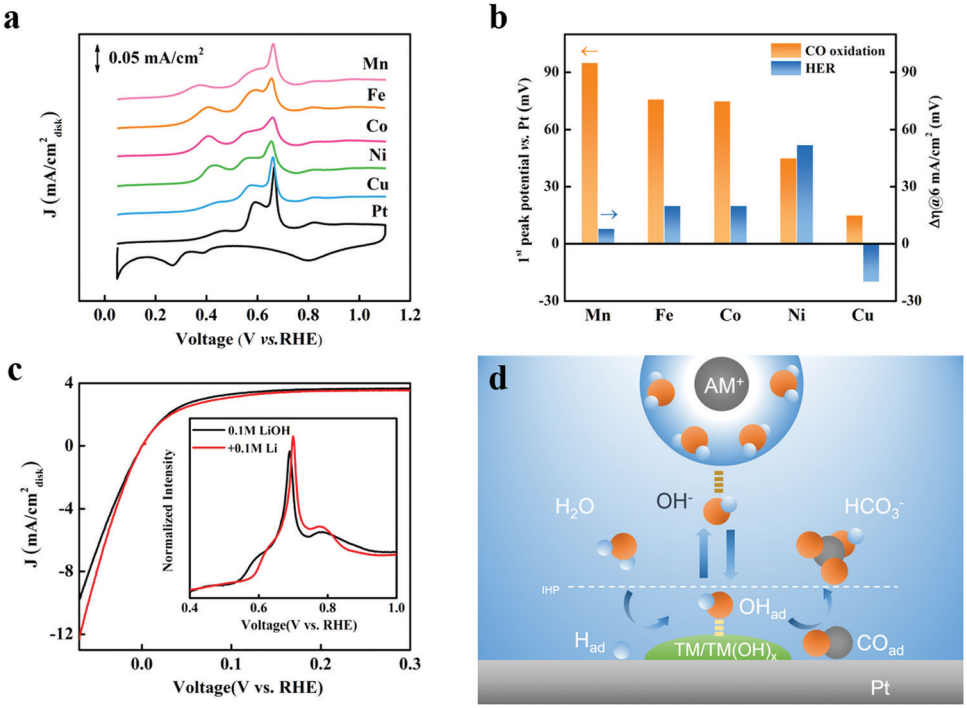

Fig. 4 (a) Voltammetric profiles of CO stripping for Pt polycrystalline in an Ar-saturated 0.1 M KOH electrolyte with/without surface deposited TM (100 μM). Scan rate: 20 mV s^{-1}. E_{ads} = 0.05 V. (b) The TM-induced HER and CO oxidation improvement of Pt polycrystalline in a H_2- and Ar-saturated 0.1 M KOH electrolyte, respectively. (TM coverage 30–40%.) $\Delta\eta$ represents the reduction of the HER overpotential when the current density reaches 6 mA cm^{-2}. TM-induced CV curves and Original HER polarization curves were given in Fig. S13 and S14 (ESI†). (c) HER polarization curves and CO stripping (inset) of Pt in 0.1 M LiOH and 0.1 M LiOH plus 0.1 M $LiClO_4$. (d) Schematic illustration of HER and CO oxidation mechanism described by eqn (5).

oxidation results but from the reverse direction. The reverse of eqn (5) is kinetically slow since it involves bringing OH^- toward the negatively charged electrode surface against the electric field. It is commonly regarded as the rds of CO oxidation of Pt in alkali,[44] followed by the reaction between OH_{ad} and CO_{ad} through the L–H mechanism. Accordingly, the surface TM with strong E_{M-O}[36,45] including Mn, Fe, Co, or Ni promotes the CO oxidation of Pt in alkali by attracting OH^- from the electrolyte forming OH_{ad}, and the improvement decreases with weaker E_{M-O}: Mn > Fe ~ Co > Ni (Fig. 4b). The Surface TMs also improve the HER of Pt in alkali by hosting the OH_{ad} generated from water dissociation to trigger the HSAB mechanism, but the improvement increases with weaker E_{M-O}: Mn < Fe ~ Co < Ni as found here (Fig. 4b) and elsewhere.[10,15] The opposite trends between the TM-induced improvement of the HER and CO oxidation kinetics of Pt with E_{M-O} can be rationalized as these two reactions are limited by the same step (eqn (5)) but opposite directions. Likewise, increasing the Li^+ concentration promotes the HER of Pt but delays the CO oxidation (Fig. 4c); because it increases the concentration of the $[Li^+(H_2O)_x]^+$ that promotes the desorption of OH_{ad} meanwhile impedes the adsorption of OH^- as per the HSAB mechanism.[14] Moreover, when switching from acid to alkaline solutions, the switch of the proton source from H_3O^+ to H_2O contributes to the slower the HER of Pt because of the energy barrier of removing the hydroxyl rather than water dissociation, and the barrier increases as the OH^- concentration in the electrolyte increases with pH. Conversely, the switch of the hydroxyl source from H_2O to OH^-, and the increasing OH^- concentration with increasing pH favors OH^- adsorption and thus CO oxidation.[46] Therefore, the CO oxidation and HER of Pt in alkaline solutions are coupled by the shuffling of hydroxyl throughout the interface *via* $[AM(H_2O)_x]^+$ (Fig. 4d). This decouples the HER of Pt with the HOR for which the H_{ad} is desorbed by $H_2O{\downarrow}_{ad}$. Although the HOR of Pt is not the reverse of the HER in alkaline solutions, they are both catalyzed by interfacial water *via* moving the reaction intermediates out to the electrolyte.

The catalytic roles of interfacial water in the HOR/HER of Pt in aqueous solutions are further examined *via* KIE studies by substituting H_2O with D_2O in the electrolyte of 0.1 M $HClO_4$ and 0.1 M KOH. The HOR kinetics of Pt in acid does not slow down significantly upon substitution of H_2O with D_2O since it is limited by the diffusion of H_2 onto the electrode (Fig. 5a). The HER rate of Pt in acid however drops markedly (Fig. 5a). This can be ascribed to the slower diffusion of D_2 than H_2 since the HER of Pt polycrystalline is limited by the mass transport of the generated H_2/D_2 to the bulk electrolyte[47] On the other hand, both the HOR/HER kinetics in 0.1 M KOH is much slower in D_2O than in H_2O (Fig. 5b), in agreement with Tang *et al.*'s recent KIE studies on the Pt(111) and Pt(110) in alkali.[48] This result indicates that either interfacial water or hydroxide participates in the rds of the HER/HOR of Pt in alkali since their masses increase upon the substitution. It thus rules out the previous argument that desorption of H_{ad} is solely governed by the E_{Pt-H} and irrelevant to OH^- or H_2O.[49] Since the participation of OH^- in the rds of the HOR of Pt in alkali is ruled out as shown above, the KIE results verify the participation of interfacial water in the rds of the HOR/HER of Pt in alkali, in support of our argument that interfacial water facilitates the HER/HOR of Pt *via* shuffling the reaction intermediates.

Discussions

The new notion that interfacial water shuffles the HER/HOR intermediates fully accounts for the various surface TM-induced changes of the HOR/HER kinetics of Pt in alkali depicted in Fig. 1f. The TM with high oxophilicity in either the form of TM^0 or $TM(OH)_x$ can improve the HER of Pt in alkali by hosting the OH_{ad} generated from water dissociation to trigger the subsequent OH_{ad} removal *via* the HSAB mechanism (eqn (5), Scheme 1c); whereas only the form of TM^0 can improve the HOR by hosting $H_2O{\downarrow}_{ad}$ that removes H_{ad} on Pt (eqn (2), Scheme 1b). The TM-induced changes of the HOR/HER kinetics of Pt in alkali are thus governed by the $TM^0/TM(OH)_x$ redox potential or E_{M-O}. The TMs with too low redox potentials or too strong E_{M-O} such as Mn, Fe, or Co are dominated by $TM(OH)_x$ within the HOR potential region and can thus only improve the HER. The TMs with moderate redox potentials located within the HOR kinetic

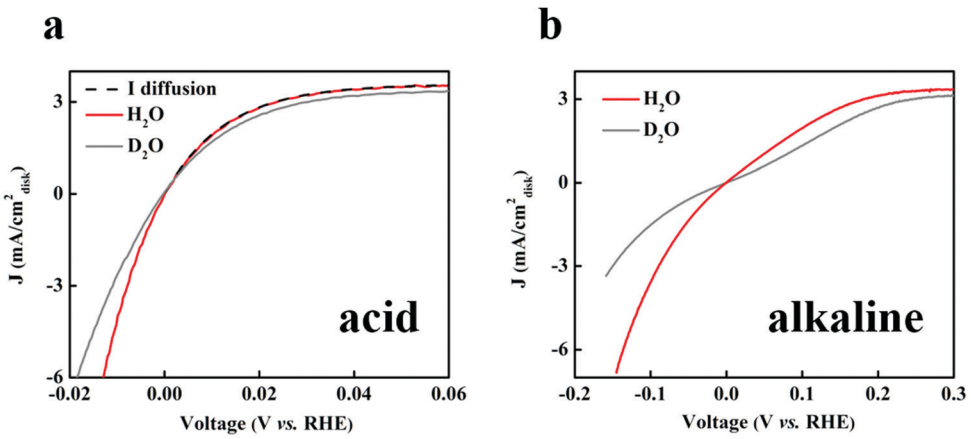

Fig. 5 The iR-corrected HOR/HER polarization curves of the Pt polycrystalline electrode in H_2-saturated 0.1 M $HClO_4$ with H_2O or D_2O (a), or in H_2-saturated 0.1 M KOH with H_2O or D_2O (b). Scan rate: 10 mV s^{-1}; rotation rate: 2500 rpm.

potential region (0–0.25 V) of Pt such as Ni and Ru can simultaneously improve the HOR/HER of Pt in alkali, but the HOR improvement vanishes as the TM^0 vanishes with increasing potentials. The higher redox potential of Ru than Ni makes the availability of Ru^0 much higher than Ni^0 for the HOR/HER (Fig. 2f), which explains why Ru improves the HOR/HER of Pt more than Ni. The TMs with high redox potentials or weak E_{M-O}(s) such as Cu improve neither. The E_{M-O} values of these TMs reported previously[36] agree well with the assignments here. By this new notion, the surface TM promotes the HOR/HER kinetics of Pt by facilitating interface water shuffling reaction intermediates against the electric field, rather than by weakening the electric field *via* negatively shifting the pzfc like lowering the pH,[11] otherwise the HOR/HER kinetics of Pt would be promoted simultaneously like lowering the pH.

In a broader context, the Pt-catalysts can be grouped into three categories: the ones that can host neither $H_2O{\downarrow}_{ad}$ nor the OH_{ad} within the HOR/HER potential region such as Pt(111)[50] (Category 1); the ones that can host OH_{ad} but not $H_2O{\downarrow}_{ad}$ such as Co@Pt (Category 2); and the ones that can host both such as Ru@Pt (Category 3) (Table S6, ESI†). In Category 1 catalysts, the $H_2O{\downarrow}$ directly reacts with the HOR/HER intermediates (H_{ad} or OH^-) through the Eley–Rideal mechanism (Scheme 1a). The reorientation of the adsorbed water molecule from lying configuration to perpendicular configuration is required for charge transfer in the Volmer step of the HER.[51] The major kinetic barrier is to bring the $H_2O{\downarrow}$ onto the surface against the interfacial electric field, part of the Volmer step. The kinetics is unaffected by AM^+,[18] and solely governed by the pH that dictates interfacial water orientation. The HOR of the Category 2 proceeds *via* the Eley–Rideal mechanism as well; whereas the HER proceeds *via* the HSAB mechanism wherein the AM^+ also plays a role (Scheme 1c). The major kinetic barrier of the HER is the removal of OH_{ad} *via* the coordinated water $[AM(H_2O)_x]^+$, but rather bringing $H_2O{\downarrow}$ onto the surface as in the Eley–Rideal mechanism. Accordingly, the dependence of the HER activity on the pH is governed by the pH-dependent concentrations of AM^+ and OH^- in the electrolyte. The HER and HOR of the Category 3 proceeds through the HSAB mechanism (Scheme 1c) and L–H mechanism (Scheme 1b), respectively. The major kinetic barrier of the L–H mechanism relies on the counterbalance between the repelling electric force on the $H_2O{\downarrow}$ and the attractive interaction between the TM^0 and $H_2O{\downarrow}$. We previously showed that the Tafel slope of the HOR of Pt/C changes from 130 mV dec^{-1} to 43 mV dec^{-1} upon the surface deposition of Ru,[20] which indicates that the strong Ru^0–$H_2O{\downarrow}$ interaction facilitates $H_2O{\downarrow}$ adsorption overcoming the electric field, thereby reducing the kinetic energy barrier. These three groups of Pt-catalysts are classified by the redox potential of the TM or the E_{M-O}, and located in the three quadrants in the Cartesian coordinate system displayed in Fig. 1f, respectively.

While interfacial water shuffles the HOR/HER intermediates *via* three different mechanisms depending on the E_{M-O}, the processes are always part of the Volmer step (Scheme 1). This underscores the importance of E_{M-O} to the Volmer step. A good HOR/HER catalyst in alkali therefore needs to possess a moderate E_{M-H} to make the Tafel step (H_2 + Pt ↔ 2Pt–H_{ad}) facile,[22] as well as a moderate E_{M-O} to make the Volmer step facile. This highlights the concept of the two-dimensional volcano trend of the HOR/HER activity in alkali proposed by Koper based on different mechanisms.[52] According to this concept, developing

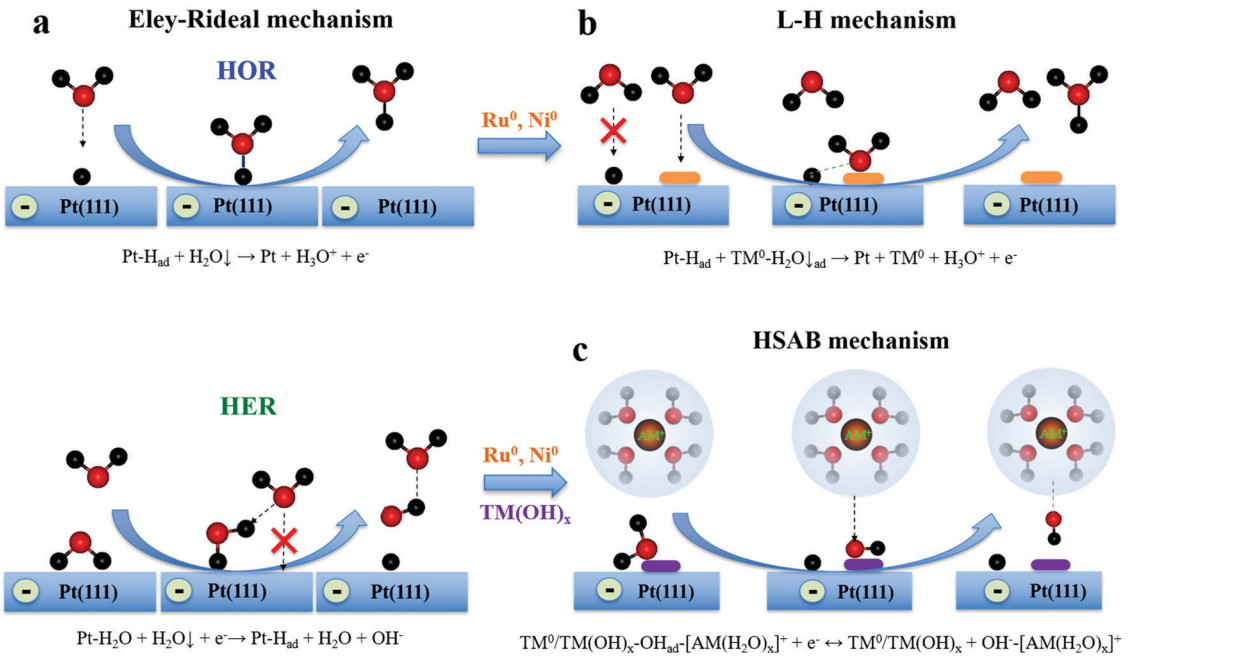

Scheme 1 (a) Schematic illustration of the Eley–Rideal mechanism of the HER/HOR of Pt(111) in alkaline solution. (b) Schematic illustration of the L–H mechanism of the HOR of TM^0@Pt in alkaline solution, wherein the yellow block represents surface TM^0 such as Ni^0 or Ru^0. (c) Schematic illustration of the HSAB mechanism of the HER of TM^0/$TM(OH)_x$@Pt in alkaline solution, wherein the purple block represents surface TM^0 such as Ni^0 or Ru^0 or $TM(OH)_x$. The red cross in (a) and (b) indicates the lack of specific adsorption or interaction, respectively.

bimetallic systems for which the E_{M-H} and E_{M-O} can be tuned separately on two different metals is a plausible strategy to design effective HOR/HER catalysts. On the other hand, the E_{M-H} and E_{M-O} are strongly correlated in monometallic systems, making it difficult to reach optimal E_{M-H} and E_{M-O} simultaneously. For example, the E_{Pt-H} is nearly optimal, whereas the E_{Pt-O} is too weak. Moreover, the competition between H_{ad} and oxygen adsorbates ($H_2O\downarrow_{ad}$ or OH_{ad}) over monometallic sites further complicates the interplay between the E_{M-H} and E_{M-O}. For instance, if the E_{M-O} is too strong, the TM such as Co or Ni[14] is nearly passivated in the form of hydroxides at 0 V where the HOR/HER exchange current is normally measured to evaluate the HOR/HER activity. As a result, this HOR/HER activity is nearly irrelevant to the E_{M-H} but governed by E_{M-O} or the redox potential that determines the availability of TM^0. Nevertheless, it was recently show that confining Ru with TiO_2 can suppress $Ru(OH)_3$ passivation, thereby dramatically improving its HOR activity.[53] This projects another strategy of developing monometallic HOR/HER catalysts by tuning E_{M-O} without affecting E_{M-H}, or *vice versa*.

3. Conclusions

In this work we revealed the critical roles of interfacial water in shuffling the HOR/HER intermediates in aqueous solutions by probing the double-layer interface *via* surface deposited transition metals, alkali metal cations, and carbon monoxide. An important merit of this notion is that the pH effect, cation effects, and surface TM effects on the HOR/HER kinetics of Pt can all be reasonably accounted for by the shuffling roles of interfacial water. Since these effects are also profound for many other reactions such as oxygen reduction/evolution reactions,[54–56] we believe the shuffling roles of interfacial water are generally the case for complicated electrochemical reactions involving multiple elementary steps in aqueous solutions.

4. Methods

Chemicals

Carbon supported platinum nanoparticles (Pt/C, 47.2 wt%) were purchased from Tanaka Kikinzoku Kogyo. Copper(II) perchlorate hexahydrate ($Cu(ClO_4)_2{\cdot}6H_2O$, 98%), nickel(II) perchlorate hexahydrate ($Ni(ClO_4)_2{\cdot}6H_2O$, 99.99%), cobalt(II) perchlorate hexahydrate ($Co(ClO_4)_2{\cdot}6H_2O$, 99%), iron(III) perchlorate hydrate ($Fe(ClO_4)_3{\cdot}H_2O$, crystalline, low chloride), manganese(II) perchlorate hydrate ($Mn(ClO_4)_2{\cdot}xH_2O$, 99%), potassium hydroxide (KOH, 99.99%), perchloric acid ($HClO_4$, 70%, PPT Grade), deuterium oxide (D_2O, 99.9% D) were all purchased from Sigma-Aldrich. All aqueous solutions were prepared using deionized (DI) water (18.2 MΩ cm) obtained from an ultra-pure purification system (Aqua Solutions).

Electrode preparation

Prior to the electrodeposition, the glassy carbon electrode embedded in PTFE or the Pt polycrystalline electrode was polished mechanically with 0.5 μm, 0.3 μm, 0.05 μm alumina powder and then sonicated in sequence for 5 minutes in DI water and ethanol.

Electrochemical measurements

All the electrochemical experiments were conducted using a three-electrode cell system. Pt wire and Ag/AgCl (1 M Cl^-) reference electrode were used as the counter and reference electrodes respectively. All potentials reported in this paper are referenced to the reversible hydrogen electrode (RHE), calibrated in the same electrolyte by measuring the potential of the HOR/HER currents at zero corresponding to 0 V *versus* RHE (V_{RHE}).

Prior to the RDE testing in alkali, the Pt polycrystalline electrode was cycled with a rotation rate of 1600 rpm in an Ar-saturated 0.1 M $HClO_4$ electrolyte with a scan rate of 500 mV s^{-1} between the potential range of 0.05–1.2 V_{RHE} for 100 cycles following the Department of Energy (DOE) recommended protocol.[57] The typical experimental procedures for HOR/HER experiments can be referred to in our previous work.[14] All polarization curves in this paper are iR-corrected.

Kinetic isotope effect (KIE) studies. The 0.1 M KOH and $HClO_4$ electrolyte with H_2O or D_2O were made by diluting high-purity KOH or $HClO_4$ with Millipore water or D_2O, respectively. All prepared electrolytes had a final concentration of 0.1 M and pH values of 13 or 1.

Impedance measurements. The impedance spectra were measured with frequencies from 10^5 to 0.1 Hz with an amplitude of 10 mV by Autolab. Equivalent circuits were fitted to the data with Zview software.

Electrochemical deposition of $M(ClO_4)_2$ (M = Mn, Co, Ni, Cu), $Fe(ClO_4)_3$ and $RuCl_3$. After the CV and HOR/HER measurements of the Pt polycrystalline, the electrode was unmounted from the RDE and immersed in 20 μM $M(ClO_4)_2$ for 1 minute. Then the HOR/HER polarization curves and the CV were recorded in a H_2/Ar-saturated 0.1 M KOH electrolyte under identical conditions as those of Pt polycrystalline. This process was repeated with increasing concentration of $M(ClO_4)_2$ until the coverage reaches the target (for HER and CO oxidation comparison). The electrochemical deposition for $RuCl_3$ followed the protocol of our previous study.[20]

CO stripping. Before conducting the CO stripping experiments, two potential cycles between 0.05 and 1.1 V_{RHE} in 0.1 M KOH with a scan rate of 20 mV s^{-1} were applied to the electrode before the adsorption of carbon monoxide. CO was purged while the working electrode was held at a constant potential of 0.05 V_{RHE} for 5 minutes, and then Ar was purged into the same electrolyte for 25 minutes at the same potential to remove the CO from the electrolyte.

***In situ* XAS data collection and analysis.** The preparation method of the XAS electrodes can be referred to in our previous work.[58] The final Pt geometric loadings were chosen to give 0.5 transmission spectra edge heights at the Pt L_3 edge. The XAS experiments were conducted at room temperature in a previously described flow half-cell in which H_2-purged 0.1 M KOH was continuously circulated. The voltage cycling limits were −0.3 to 0.6 V_{RHE} or 1 V_{RHE} for Ru/C. The data at the K-edge of the TM in TM@Pt except for Ru@Pt were collected in the

fluorescence mode at the beamline ISS 8-ID, the data at the Ru K-edge of Ru-based samples were collected in 7-BM and the data of RuO_2 standard were collected in 6-BM of the National Synchrotron Light Source (NSLS) II, Brookhaven National Laboratory (BNL). Typical experimental procedures were utilized with details provided in our previous work.[58]

Author contributions

Q. J. conceived the project. Q. J. conceived and designed the *in situ* XAS experiments and electrochemical experiments. E. L. conducted all the electrochemical experiments and analyzed the data. Q. J. and S. M. supervised and advised the electrochemical experiments and data analysis. E. L., Q. J., J. L., L. J., Q. S., and T. S. conducted the *in situ* XAS experiments. Q. J. analyzed the XAS data. Q. J. and E. L. derived the new notion. Q. J., E. L., and T. S. wrote the manuscript.

Conflicts of interest

The authors declare no competing financial interests.

Acknowledgements

This work was supported by the Office of Naval Research (ONR) under award number N00014-18-1-2155 and the Graduate Thesis/Dissertation Grant of Northeastern University, Massachusetts, 02115, United States. This research used beamline 6-BM, 7-BM (QAS) and 8-ID (ISS) of the National Synchrotron Light Source II, a U.S. Department of Energy (DOE) Office of Science User Facility operated for the DOE Office of Science by Brookhaven National Laboratory under Contract No. DE-SC0012704. Beamline operations were supported in part by the Synchrotron Catalysis Consortium (U.S. DOE, Office of Basic Energy Sciences, Grant No. DE-SC0012335).

References

1 T. Erdey-Gruz and M. Volmer, *Z. Phys. Chem.*, 1930, **150**, 203.
2 S. Trasatti, *J. Electroanal. Chem. Interfacial Electrochem.*, 1972, **39**, 163–184.
3 E. Skúlason, V. Tripkovic, M. E. Björketun, S. Gudmundsdóttir, G. Karlberg, J. Rossmeisl, T. Bligaard, H. Jónsson and J. K. Nørskov, *J. Phys. Chem. C*, 2010, **114**, 18182–18197.
4 J. Herranz, J. Durst, E. Fabbri, A. Patru, X. Cheng, A. A. Permyakova and T. J. Schmidt, *Nano Energy*, 2016, **29**, 4–28.
5 W. Sheng, Z. Zhuang, M. Gao, J. Zheng, J. G. Chen and Y. Yan, *Nat. Commun.*, 2015, **6**, 1–6.
6 J. Zheng, W. Sheng, Z. Zhuang, B. Xu and Y. Yan, *Sci. Adv.*, 2016, **2**, e1501602.
7 J. Zheng, J. Nash, B. Xu and Y. Yan, *J. Electrochem. Soc.*, 2018, **165**, H27–H29.
8 T. Cheng, L. Wang, B. V. Merinov and W. A. Goddard, *J. Am. Chem. Soc.*, 2018, **140**, 7787–7790.
9 D. Strmcnik, M. Uchimura, C. Wang, R. Subbaraman, N. Danilovic, D. Van Der Vliet, A. P. Paulikas, V. R. Stamenkovic and N. M. Markovic, *Nat. Chem.*, 2013, **5**, 300–306.
10 R. Subbaraman, D. Tripkovic, K.-C. Chang, D. Strmcnik, A. P. Paulikas, P. Hirunsit, M. Chan, J. Greeley, V. Stamenkovic and N. M. Markovic, *Nat. Mater.*, 2012, **11**, 550–557.
11 I. Ledezma-Yanez, W. D. Z. Wallace, P. Sebastián-Pascual, V. Climent, J. M. Feliu and M. T. M. Koper, *Nat. Energy*, 2017, **2**, 17031.
12 M. J. Van der Niet, N. Garcia-Araez, J. Hernández, J. M. Feliu and M. T. Koper, *Catal. Today*, 2013, **202**, 105–113.
13 T. J. Schmidt, P. N. Ross and N. M. Markovic, *J. Electroanal. Chem.*, 2002, **524–525**, 252–260.
14 E. Liu, J. Li, L. Jiao, H. T. T. Doan, Z. Liu, Z. Zhao, Y. Huang, K. M. Abraham, S. Mukerjee and Q. Jia, *J. Am. Chem. Soc.*, 2019, **141**, 3232–3239.
15 L. Rebollar, S. Intikhab, J. D. Snyder and M. H. Tang, *J. Electrochem. Soc.*, 2018, **165**, J3209–J3221.
16 N. Danilovic, R. Subbaraman, D. Strmcnik, A. P. Paulikas, D. Myers, V. R. Stamenkovic and N. M. Markovic, *Electrocatalysis*, 2012, **3**, 221–229.
17 R. Subbaraman, D. Tripkovic, D. Strmcnik, K.-C. Chang, M. Uchimura, A. P. Paulikas, V. Stamenkovic and N. M. Markovic, *Science*, 2011, **334**, 1256–1260.
18 D. Strmcnik, K. Kodama, D. van der Vliet, J. Greeley, V. R. Stamenkovic and N. M. Marković, *Nat. Chem.*, 2009, **1**, 466.
19 S. Intikhab, L. Rebollar, X. Fu, Q. Yue, Y. Li, Y. Kang, M. H. Tang and J. D. Snyder, *Nano Energy*, 2019, **64**, 103963.
20 J. Li, S. Ghoshal, M. K. Bates, T. E. Miller, V. Davies, E. Stavitski, K. Attenkofer, S. Mukerjee, Z.-F. Ma and Q. Jia, *Angew. Chem., Int. Ed.*, 2017, **56**, 15594–15598.
21 Q. Jia, S. Ghoshal, J. Li, W. Liang, G. Meng, H. Che, S. Zhang, Z.-F. Ma and S. Mukerjee, *J. Am. Chem. Soc.*, 2017, **139**, 7893–7903.
22 W. Sheng, M. Myint, J. G. Chen and Y. Yan, *Energy Environ. Sci.*, 2013, **6**, 1509–1512.
23 A. N. Kuznetsov, A. G. Oshchepkov, O. V. Cherstiouk, P. A. Simonov, R. R. Nazmutdinov, E. R. Savinova and A. Bonnefont, *ChemElectroChem*, 2020, **7**, 1438–1447.
24 J. Juodkazytė, R. Vilkauskaitė, G. Stalnionis, B. Šebeka and K. Juodkazis, *Electroanalysis*, 2007, **19**, 1093–1099.
25 Y. Sugawara, A. Yadav, A. Nishikata and T. Tsuru, *J. Electrochem. Soc.*, 2008, **155**, B897–B902.
26 I. Povar and O. Spinu, *J. Electrochem. Sci. Eng.*, 2016, **6**, 145–153.
27 S. Alayoglu, P. Zavalij, B. Eichhorn, Q. Wang, A. I. Frenkel and P. Chupas, *ACS Nano*, 2009, **3**, 3127–3137.
28 S. D. Kelly, K. M. Kemner, J. B. Fein, D. A. Fowle, M. I. Boyanov, B. A. Bunker and N. Yee, *Geochim. Cosmochim. Acta*, 2002, **66**, 3855–3871.
29 J. M. Mayer, *Inorg. Chem.*, 1988, **27**, 3899–3903.
30 P. J. Feibelman, *Science*, 2002, **295**, 99–102.
31 M. Tatarkhanov, E. Fomin, M. Salmeron, K. Andersson, H. Ogasawara, L. G. M. Pettersson, A. Nilsson and J. I. Cerdá, *J. Chem. Phys.*, 2008, **129**, 154109.
32 A. Michaelides, A. Alavi and D. A. King, *J. Am. Chem. Soc.*, 2003, **125**, 2746–2755.

33 J. N. Schwämmlein, B. M. Stühmeier, K. Wagenbauer, H. Dietz, V. Tileli, H. A. Gasteiger and H. A. El-Sayed, *J. Electrochem. Soc.*, 2018, **165**, H229–H239.
34 K. Elbert, J. Hu, Z. Ma, Y. Zhang, G. Chen, W. An, P. Liu, H. S. Isaacs, R. R. Adzic and J. X. Wang, *ACS Catal.*, 2015, **5**, 6764–6772.
35 W. Liu, K. Lyu, L. Xiao, J. Lu and L. Zhuang, *Electrochim. Acta*, 2019, **327**, 135016.
36 J. K. Nørskov, J. Rossmeisl, A. Logadottir, L. Lindqvist, J. R. Kitchin, T. Bligaard and H. Jónsson, *J. Phys. Chem. B*, 2004, **108**, 17886–17892.
37 W. Sheng, H. A. Gasteiger and Y. Shao-Horn, *J. Electrochem. Soc.*, 2010, **157**, B1529–B1536.
38 J. Ryu and Y. Surendranath, *J. Am. Chem. Soc.*, 2019, **141**, 15524–15531.
39 K.-i. Ataka, T. Yotsuyanagi and M. Osawa, *J. Phys. Chem.*, 1996, **100**, 10664–10672.
40 N. Ramaswamy, S. Ghoshal, M. K. Bates, Q. Jia, J. Li and S. Mukerjee, *Nano Energy*, 2017, **41**, 765–771.
41 N. M. Marković and P. N. Ross, *Surf. Sci. Rep.*, 2002, **45**, 117–229.
42 M. Watanabe and S. Motoo, *J. Electroanal. Chem. Interfacial Electrochem.*, 1975, **60**, 267–273.
43 S. Intikhab, J. D. Snyder and M. H. Tang, *ACS Catal.*, 2017, **7**, 8314–8319.
44 T. J. Schmidt, P. N. Ross and N. M. Markovic, *J. Phys. Chem. B*, 2001, **105**, 12082–12086.
45 R. B. Rankin and J. Greeley, *ACS Catal.*, 2012, **2**, 2664–2672.
46 G. García, *ChemElectroChem*, 2017, **4**, 459–462.
47 J. Zheng, Y. Yan and B. Xu, *J. Electrochem. Soc.*, 2015, **162**, F1470–F1481.
48 L. Rebollar, S. Intikhab, J. D. Snyder and M. H. Tang, *J. Phys. Chem. Lett.*, 2020, **11**, 2308–2313.
49 J. Durst, A. Siebel, C. Simon, F. Hasché, J. Herranz and H. A. Gasteiger, *Energy Environ. Sci.*, 2014, **7**, 2255–2260.
50 I. T. McCrum and M. J. Janik, *J. Phys. Chem. C*, 2016, **120**, 457–471.
51 O. Pecina and W. Schmickler, *Chem. Phys.*, 1998, **228**, 265–277.
52 M. T. M. Koper, *Nat. Chem.*, 2013, **5**, 255–256.
53 Y. Zhou, Z. Xie, J. Jiang, J. Wang, X. Song, Q. He, W. Ding and Z. Wei, *Nat. Catal.*, 2020, **3**, 454–462.
54 J.-W. Zhao, C.-F. Li, Z.-X. Shi, J.-L. Guan and G.-R. Li, *Research*, 2020, 6961578.
55 Y. Chen, T. Cheng and W. A. Goddard III, *J. Am. Chem. Soc.*, 2020, **142**, 8625–8632.
56 J. Staszak-Jirkovský, R. Subbaraman, D. Strmcnik, K. L. Harrison, C. E. Diesendruck, R. Assary, O. Frank, L. Kobr, G. K. H. Wiberg, B. Genorio, J. G. Connell, P. P. Lopes, V. R. Stamenkovic, L. Curtiss, J. S. Moore, K. R. Zavadil and N. M. Markovic, *ACS Catal.*, 2015, **5**, 6600–6607.
57 S. S. Kocha, K. Shinozaki, J. W. Zack, D. J. Myers, N. N. Kariuki, T. Nowicki, V. Stamenkovic, Y. Kang, D. Li and D. Papageorgopoulos, *Electrocatalysis*, 2017, **8**, 366–374.
58 Q. Jia, W. Liang, M. K. Bates, P. Mani, W. Lee and S. Mukerjee, *ACS Nano*, 2015, **9**, 387–400.

